




Shape memory polymers as actuators: Characterization of the relevant parameters under constrained recovery

Carina Peixoto¹ | Andrea Zille²  | Alexandre Ferreira da Silva³  |
Olga Sousa Carneiro¹ 

¹IPC—Institute for Polymers and Composites, University of Minho, Guimarães, Portugal

²2C2T—Center for Science and Textile Technology, University of Minho, Guimarães, Portugal

³CMEMS—Center for MicroElectroMechanical Systems, University of Minho, Guimarães, Portugal

Correspondence

Olga Sousa Carneiro, Polymer Engineering Department, Campus de Azurém, Universidade do Minho, 4800-085 Guimarães, Portugal.
Email: olgasc@dep.uminho.pt

Funding information

Fundação para a Ciência e a Tecnologia, Grant/Award Numbers: UIDB/04436/2020, UIDP/04436/2020, UIDB/05256/2020, UIDP/05256/2020

Abstract

In this work, a shape memory polyurethane is characterized through constrained recovery experiments performed in a tensile testing equipment. The most relevant results obtained are those concerned with the stress released over time during the recovery stage, since they provide quantitative information that can be used in the design of actuators. For this sake, design guidelines are proposed based on the effect of: (i) the programming temperature; (ii) the deformation imposed during the programming stage; (iii) the recovery temperature; and (iv) the manufacturing process used to produce the samples tested (compression molding and Fused Filament Fabrication). The set of experiments performed with compression-molded samples put in evidence a considerable variety of material responses: (i) the maximum released stress varied from 0.74 to 1.68 MPa; (ii) the time required to attain this stress varied from 47 to 600 s; and (iii) the stress was released as a peak value that relaxed rapidly, or, contrarily, had a lasting effect. Another relevant conclusion is that the 3D printing technique does not affect the shape memory behavior of the material. Having this in mind, the conclusions provided by the compression-molded samples study can be extended to printed ones.

KEYWORDS

4D printing, constrained recovery, fused filament fabrication, polyurethane, shape memory polymers

1 | INTRODUCTION

Shape Memory Polymers (SMP) are mechanically active materials, i.e., capable of altering their shape as a response to an external stimulus. This type of materials memorizes an original/permanent shape, has the ability to store a temporary shape (after being deformed) and, later, to recover the permanent shape when subjected to the adequate stimulus.^[1] Temperature is one of the most commonly used and studied stimuli, and the SMP sensitive to this kind of stimulus are called thermosensitive. When compared to other shape memory materials, namely shape memory alloys, SMP present several interesting characteristics, namely:

high deformation capability (up to 800%), low cost, low density, biocompatibility, and biodegradability.^[2,3] Furthermore, they are easy to process, and their application temperatures can be adjusted. This set of characteristics make SMP potential candidates for application in different areas such as biomedical,^[4] textile,^[5] aerospace,^[6] and automotive, both as sensors and actuators, among others.

The shape memory behavior can be observed in several polymers, which may have different chemical structures.^[7–10] In these materials, the molecular mechanism responsible for the memory effect is related with the existence of crosslinking bonds (physical or chemical), that assures the permanent shape, and the existence of flexible

segments, which acts as the reversible phase and enables the creation of the temporary shape. Several approaches have been successfully proposed to improve shape memory properties in polyurethanes, by varying the nature and the ratio of their flexible segments.^[11,12] However, shape memory is not an intrinsic property of the material but a result of its molecular structure, processing technique used to produce the permanent shape, and programming method applied.^[7] Thus, it is essential to study the parameters related to the processing and programming stages in order to potentiate its performance and to be able to predict its behavior during recovery.

When used as smart materials, SMP are able to detect the specific external stimulus required to change their shape or to release their internal energy (when the shape change is hindered). For this reason, SMP have been characterized under two different conditions: (i) free recovery, which occurs when there are no forces being applied to the SMP samples during the recovery stage. In this case, the sample recovers partially or totally its permanent shape; and (ii) constrained recovery, which occurs whenever the recovery is hindered. In this case, the stress generated by the material during the recovery stage can be monitored.^[13]

The majority of publications on SMP is focused on the synthesis of these materials, and on the characterization of their transition temperatures, carried out in free or constrained recovery experiments. However, recovery over time, especially in constrained recovery conditions, has not been extensively studied, and some applications require recovery under isothermal conditions.^[14,15]

Combining the SMP capability of changing shape/generating stresses over time and the unique potential of 3D printing to produce complex shape parts, the so-called 4D printing, new applications can be envisaged. In the last few years, several authors have been investigating the potential of SMP for 3D printing. In this context, Bodaghi et al. developed constitutive models and numerical codes to predict the impact behavior of SMP beams,^[16] the behavior of meta-structures,^[17] and the self-bending of SMP beams printed at different speeds.^[18] Raasch et al.^[19] and Garcia Rosales et al.^[20] studied the extrusion of filament and printing conditions of SMP aiming at optimizing the shape recovery of printed samples. They concluded that it is possible to attain recovery ratios of the order of 80–90%. In recent publications, Yamamura et al.^[21] and Keneth et al.^[22] explored and illustrated the potential of using two different SMP in the same multi-material printed part, developing a hybrid hinge structure and a reversible opening and closing valve, respectively. In both cases, the researchers used a pair of materials having different transition temperatures. A wide range of applications of SMP in parts produced by fused filament fabrication (one of the most popular 3D printing techniques) can be found in a review paper from 2021.^[23]

Nonetheless, most of the referred works do not characterize the recovery behavior of the material over time, and when this is the case, it is often the strain evolution that is monitored. Recent examples of this can be found in refs [24–26]. In ref. [24], a comprehensive study on the effects of programming strain, end load and chemical environment, performed with a chemically stimulated linear SMP, is carried out; in refs [25,26] the authors studied the effect of some printing parameters and orientation of the applied stress, on the recovery behavior of cubes of PLA produced by FFF.

As a conclusion, the characterization of SMP behavior under constrained recovery is rarely addressed. However, the information provided by this type of tests is essential in the development of actuators, which are effective through the stress released when subjected to the appropriate external stimulus. This is the motivation of the present research work, which aims at investigating the influence of the programming parameters, recovery parameters, and processing technology used in the production of tensile test samples, in the constrained recovery of a commercial polyurethane. The variables studied are: (i) the programming temperature (T_{prog}); (ii) the maximum applied deformation (ϵ_m); (iii) the recovery temperature (T_{rec}); and (iv) the processing technology used to manufacture the samples, through the comparison between compression molded and printed by the Fused Filament Fabrication (FFF) samples. The final purpose is to provide relevant quantitative data and guidelines for the design of new applications employing SMP parts produced by conventional molding techniques or by 3D printing.

2 | SHAPE MEMORY POLYURETHANES

Among the several polymers with shape memory potential, thermoplastic shape memory Polyurethanes (SMPU), are considered the most attractive, presenting a vast range of processing conditions and high chemical versatility. These materials present a two-phase heterogeneous structure, composed of rigid and flexible segments.^[27] The rigid segments are formed by di-isocyanate and small molecules of glycol. These segments are characterized by strong hydrogen-urethane bonds that form physical entanglements, which act as physical cross-links. The flexible segments are polyol chains, typically polyether or polyester.^[7,28,29] The main difference between these two types of segments is their polarity that makes them thermodynamically incompatible, causing phase separation. This separation is essential for the shape memory behavior. In the case of quasi total phase separation, the activation temperature is the glass transition temperature of the flexible segments (T_g).

In order to obtain good shape memory properties, the percentage of rigid segments must be high enough to hinder molecular chains slippage.^[30] Physical cross-linking, required for shape recovery, will only be effective above a critical percentage of rigid domains.^[31,32] Polyurethanes have excellent chemical properties and biocompatibility, but present relatively low recovery stresses, being used in applications where low forces are required.^[33,34]

In this work, a commercially available thermosensitive shape memory polyurethane (PU) was used. There are some publications reporting its behavior in free recovery experiments, performed under different conditions, that demonstrate its good shape memory properties, namely a recovery ratio, R_r of around 80%–90%.^[35–39]

3 | METHODOLOGY FOR SMP CHARACTERIZATION

3.1 | Thermo-mechanical cycle

Several tests used to quantify the macroscopic properties of shape memory polymers systems have been reported in the literature, namely, thermomechanical tensile tests,^[40–42] three-point flexural tests for composites^[43,44] and compression tests for cellular materials.^[45]

The thermomechanical tensile tests are the most popular and their main stages (programming, fixing and recovery) and variants (free and constrained recovery) are illustrated in Figure 1.

The programming stage can be carried out in controlled deformation mode, where the maximum deformation applied (ϵ_m) and the deformation rate ($\dot{\epsilon}$) are set, or in controlled stress mode, where the applied stress (σ) is set. The values selected for these parameters

may have a significant impact on the polymer behavior.^[30] These tests are normally conducted in a conventional tensile testing machine, equipped with a thermal chamber, which enables the temperature control during the deformation and recovery stages of the sample. In alternative, a dynamic mechanical analysis equipment (DMA) may be used in tensile^[46,47] or flexural^[14,48,49] modes.

The effectiveness of programming may be quantified by the shape fixation ratio (R_f), defined by Equation (1). This parameter is extremely relevant in this context since it describes the capability of the flexible segments to fix the mechanical deformation (temporary shape) promoted during the programming stage. This ratio is computed through the deformation measured after sample cooling and stress removal (ϵ_u) and the maximum deformation applied (ϵ_m)^[7]:

$$R_f = \frac{\epsilon_u}{\epsilon_m}. \quad (1)$$

In constrained recovery mode, the deformation is maintained constant ($\epsilon(t) = \epsilon_m = \text{const}$) in isothermal conditions or at a specific heating rate.^[50] In this type of test, the recovery force/stress, resulting from the stored energy during the programming stage, is monitored over time. The stored energy depends on the conditions in which programming was carried out, namely, maximum deformation (ϵ_m), maximum stress applied (σ_m), deformation rate ($\dot{\epsilon}$) and programming temperature (T_{prog}). The majority of the published works studied the influence of the programming parameters on the free recovery behavior as, for example, Schmidt et al.,^[35] Santiago et al.,^[36] and Tobushi et al.^[42] Gall et al.^[14] studied both free and constrained recovery as a function of temperature.

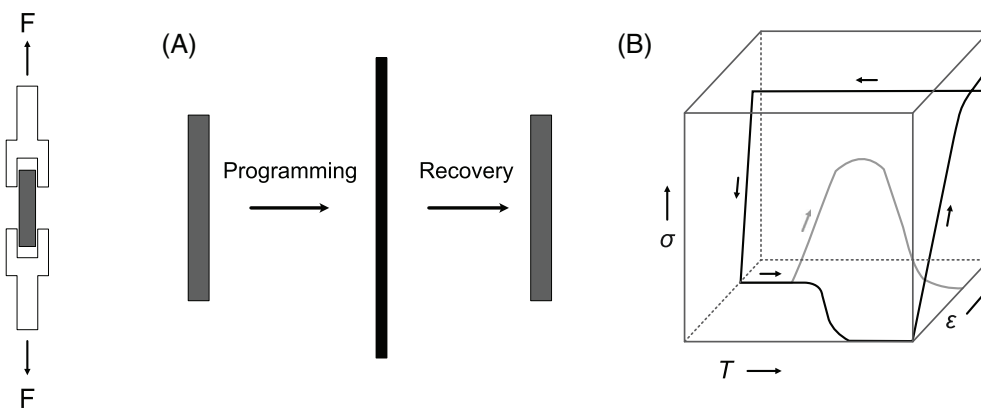


FIGURE 1 Thermo-mechanical tensile tests of SMP: (A) permanent shape (in gray) and temporary shape (in black); (B) ϵ - T - σ diagram, where the black curve shows the complete test cycle, including programming (fixing) and recovery, for the free recovery case, and the gray curve shows the constrained recovery (adapted from ref. ^[13])

In this work, tensile tests in constrained recovery mode were carried out. Programming of the temporary shape was performed in controlled deformation mode, applying a maximum deformation, ϵ_m , in isothermal conditions, at T_{prog} . For this sake, samples were conditioned in the heating chamber for 10 min before starting the test. Young's modulus (E) and the stress required to attain the set deformation, $\sigma(\epsilon_m)$, were determined through the corresponding stress-deformation curves obtained.

After deformation of the samples (up to the temporary shape), they were cooled down by air forced convection until T_{fix} , maintaining ϵ_m constant. This temperature must be lower than the on-set transition temperature ($T_{fix} < T_{onset}$) of the material,^[51] and the cooling process should be fast, in order to minimize the extent of material relaxation processes. The stress-deformation curve was also acquired during this stage, being the stress remaining after cooling (residual stress) taken as the maximum stress, σ_m . The unloading stage must occur after the cooling stage, i.e. at a sample temperature of T_{fix} , in order to minimize/avoid eventual free recovery of the deformed sample. Unloading consisted in releasing the sample from the jaws of the tensile testing equipment. The time interval corresponding to the programming and fixing stages is the storage time, τ_r , and was set to 600 s. The stages above described were maintained for all the conditions studied.

At the constrained recovery stage, the imposition of a small deformation (0.2%) was required to initiate the data acquisition process. This stage was performed at the recovery temperature, T_{rec} . The maximum recovery stress ($\sigma_{R,max}$) and the corresponding time ($t_{\sigma_{R,max}}$) were registered and the shape of the stress-time curve was analyzed. To characterize the recovery stage, the following ratios, related to the stress conversion, were considered^[51]:

– between the maximum recovery stress and the stress applied in the programming stage,

$$\sigma_{R,max}/\sigma_{(\epsilon)} \tag{2}$$

– between the maximum recovery stress and the residual stress that remained in the deformed sample after cooling,

$$\sigma_{R,max}/\sigma_m \tag{3}$$

The sequence of stages corresponding to a complete thermo-mechanical cycle are illustrated in Figure 2 and summarized as follows:

1. *Programming of the temporary shape*: imposing a deformation ϵ_m at T_{prog} , using a predefined deformation rate ($\dot{\epsilon}$);
2. *Fixing the temporary shape*: cooling down until T_{fix} , maintaining the applied deformation (ϵ_m) constant;
3. *Unloading*: releasing the sample from the jaws ($\sigma = 0$), maintaining the sample at T_{fix} during $\tau_r = 600$ s;
4. *Constrained recovery*: setting the heating chamber at T_{rec} , placing the sample into the jaws and measuring the recovery stress (σ_{rec}) over time.

3.2 | Parameters studied

In the present study, the following parameters were varied: (i) programming stage—temperature, and applied deformation; (ii) recovery stage—temperature; and (iii) manufacturing process used to produce the samples—compression molding and 3D Printing (FFF). The reference testing conditions were as follows: programming and recovery temperatures set at T_{trans} , an applied maximum deformation of 100% (value limited by the equipment characteristics), and compression molding as the manufacturing process. The determination of T_{trans} is described in the next section and the set of experiments performed are summarized in Table 1.

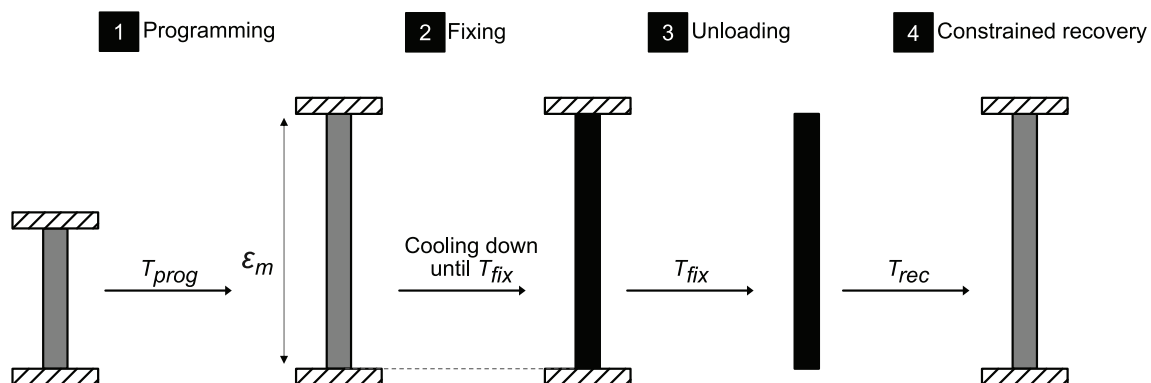


FIGURE 2 Sequence of the thermo-mechanical cycle used to characterize the constrained recovery of samples along time: 1—programming; 2—fixing; 3—Unloading; 4—constrained recovery (after heating the chamber)

TABLE 1 Parameters studied

Objective	Programming		Recovery	
	T_{prog}	ϵ_m (%)	T_{rec}	
Influence of the programming temperature (T_{prog})	$T_{\text{prog}} < T_{\text{trans}}$	100	$T_{\text{rec}} \approx T_{\text{trans}}$	
	$T_{\text{prog}} \approx T_{\text{trans}}$			
	$T_{\text{prog}} > T_{\text{trans}}$			
Influence of the maximum deformation (ϵ_m)	$T_{\text{prog}} \approx T_{\text{trans}}$	25	$T_{\text{rec}} \approx T_{\text{trans}}$	
		50		
		75		
		100		
Influence of the recovery temperature (T_{rec})	$T_{\text{prog}} \approx T_{\text{trans}}$	100	$T_{\text{rec}} < T_{\text{trans}}$	
			$T_{\text{rec}} \approx T_{\text{trans}}$	
			$T_{\text{rec}} > T_{\text{trans}}$	
Influence of the manufacturing process	Compression molding	$T_{\text{prog}} \approx T_{\text{trans}}$	100	$T_{\text{rec}} \approx T_{\text{trans}}$
	3D Printing			

4 | MATERIAL AND EXPERIMENTAL METHODS

4.1 | Material

The material used was *Tecoflex*[®] (TFX EG-72D, from Lubrizol, USA), a medical grade for extrusion and injection molding, supplied in the pellet form. *Tecoflex*[®] is a cyclic aliphatic PU with polyether (PEU) base, synthesized from methylene bis(p-cyclohexyl isocyanate) (H_{12} MDI), 1,4-butanediol (1,4-BD), and poly(tetramethylene ether glycol) (PTMEG)^[52].

Hydrogen bonding has an important role in the properties of this type of materials. In this case, hydrogen bonds occur between rigid segments (H_{12} MDI and 1,4-BD), and rigid and flexible segments (H_{12} MDI/PTMEG), leading to crosslinking. In this way, micro-phase-separated morphologies are formed, namely, rigid segments immersed in a flexible segment matrix. As reported in the literature, this mixed phase material exhibits a glass transition temperature, T_{trans} , between 20 and 90°C, i.e., in the range of the glass transition temperatures of the rigid and flexible segments.^[35,37,38,53] Due to the wide range reported and in order to get a reliable value, it was decided to characterize this temperature using two different techniques (Differential Scanning Calorimetry, DSC, and Dynamic Mechanical Analysis, DMA).

DSC tests were performed in a *DSC Netzsch 200F3*, in inert atmosphere (N_2). Before the measurement, the thermal history of the sample was removed via a heating stage performed up to 180°C, at a heating rate of 20°C/min, followed by a cooling stage until 30°C at a cooling rate of 10°C/min. The second heating stage was done

from this temperature until 180°C, at a heating rate of 10°C/min. Figure 3A shows the curve corresponding to the second heating stage. As it can be seen, T_g is around 51°C.

Other endothermic peaks can be observed in the range 80–120°C, characteristic of this type of materials,^[54,55] corresponding to the dissociation of hydrogen bonds existing in the rigid segments of the PEU structure and melting of the rigid segments.^[56,57] In practical applications, the melting temperature should not be attained in order to preserve the material structure and its shape memory capability.

DMA technique is very sensitive to molecular chain movements and, therefore, suitable to determine T_g ^[58], being an alternative to DSC. In this case, a *Hitachi High-Tech Sciences* (DMA-7100) was used, in three-point flexural test mode. Samples with 40 × 15 × 3.2 mm were produced by compression molding. The tests were performed from 22 to 130°C (heating rate of 2°C/min), at a frequency of 1 Hz and applying static and dynamic forces of 50 mN and 40 nM, respectively. The curves obtained for the storage modulus (E') and $\tan \delta$, as a function of temperature, are shown in Figure 3B. In this figure, two alternative ways of determining T_g are also shown, namely T_{onset} , around 46°C, corresponding to the beginning of the transition, and $T_{\delta, \text{max}}$, around 56°C, corresponding to the $\tan \delta$ curve peak.

The low values of $\tan \delta$, between 0.2 and 0.7, demonstrate a predominant elastic behavior of the material, due to the hydrogen bonds crosslinking, characteristic of shape memory materials.

In a previous work performed with the same material, a higher value for the transition temperature (74°C) was

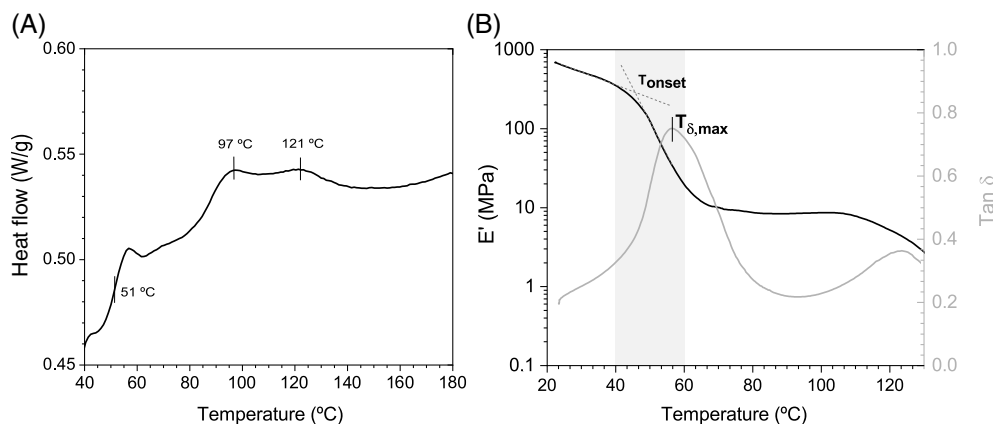


FIGURE 3 Characterization of T_g : (A) DSC second heating curve; (B) DMA tests showing the transition temperature of the material as determined by two different processes

found,^[35] being the difference associated with the higher frequency used in the DMA tests performed.^[52] According to Yakacki et al.^[59] and having in mind all the results obtained in the present work, T_{trans} was taken as 50°C and constitutes the reference value for the programming and recovery temperatures. In the thermo-mechanic tests, the values adopted for these two temperatures are those shown in Table 2. This additional information completes that given in Table 1.

4.2 | Samples production

The majority of the samples used in the characterization of the shape memory behavior were produced by compression molding, in a *Moore* hot-plate press. The material was previously dried in an oven for 2 h at 66°C, as recommended by the supplier. Sheets of 4 mm thickness were produced in the following conditions: 5 min of pre-heating at 200°C, followed by 10 min of compression at 20 TON, and finally cooling under pressure until 30°C. These sheets were subsequently laser cut into the final dimensions (80 × 10 × 4 mm).

In order to produce 3D-printed samples, the extrusion of filament from the available pellets was required. This was carried out in an extrusion line described elsewhere,^[60,61] in the conditions listed in Table 3. Pre-drying of the material was done before extrusion, in the conditions already described.

The equipment used to print samples similar to those produced by compression molding was an open source Prusa i3. The extruded filament was again pre-dried before printing. The filling degree used was 100%, in order to mimic as much as possible the compactness of the molded samples, and the printing orientation (+45°/−45°) was selected to minimize the samples anisotropy. The main printing parameters are listed in Table 4.

TABLE 2 Values selected for the programming and recovery temperatures, after material characterization, which complete the information given in Table 1

Programming/recovery temperatures	Value (°C)
$T < T_{trans}$	40
$T \approx T_{trans}$	50
$T > T_{trans}$	60

TABLE 3 Operating conditions used in the extrusion of Tecoflex filament

Parameter	Value
Extruder barrel temperature profile (°C)	170–180
Extrusion die temperature (°C)	180
Screw speed (rpm)	10.5
Pulling rolls speed (m/min)	3.5

TABLE 4 Printing conditions used in the production of samples

Parameter	Value
Layer height (mm)	0.2
Filing degree (%)	100
Printing orientation (°)	±45
Nozzle diameter (mm)	0.4
Printing speed (mm/min)	1450
Bed temperature (°C)	40
Extrusion temperature (°C)	220

4.3 | Constrained recovery tests

The methodology used was described in detail in Section 3, in the conditions depicted in Tables 1 and 4. The tests were carried out in a universal testing machine

SHIMADZU AG-X, illustrated in Figure 4, equipped with a load cell of 1 kN, and a heating chamber.

In order to better control/monitor the sample temperature before and during testing, two thermocouples were installed in its vicinity. The tests started when the monitored values showed an absolute variation of less than 1°C around the set temperature. Furthermore, samples were pre-conditioned inside the heating chamber at the programming temperature during, at least, 10 min. The initial length of the samples was 50 mm, and a tensile test speed, 10 mm/min.

Figure 4B,C show the sample in its original (permanent shape), i.e., before the programming stage, and after the constrained recovery stage, respectively.

5 | RESULTS, DISCUSSION, AND DESIGN GUIDELINES

In this section, the results obtained in the constrained recovery tests are shown and discussed. Whenever the value of some of the conditions employed in these tests are not referred, the reference values should be assumed, namely: $T_{\text{prog}} = 50^{\circ}\text{C}$ ($= T_{\text{trans}}$); $\epsilon_m = 100\%$; $T_{\text{rec}} = 50^{\circ}\text{C}$ (T_{trans}); compression molding as the sample manufacturing process.

5.1 | Influence of the programming temperature

In this set of tests, the programming temperature was varied, assuming values of 40, 50, and 60°C (see Tables 1

and 3). Figure 5 shows the evolution of the stress-deformation curves during the programming stage (Figure 5A), and the stress applied during the programming stage and its relaxation during the fixing stage, along time (Figure 5B), corresponding to the different programming temperatures tested.

As expected, the lower the programming temperature, the higher the stress required to deform the sample. The main difference is observed at 40°C, a temperature lower than T_{trans} , at which the molecular freedom is inhibited.

During the fixing stage, the stress relaxation phenomenon, typical of viscoelastic materials, is observable, consisting in a progressive loss of energy associated to the viscous component of the material behavior. The stress obtained after cooling is the one stored in the sample (σ_m), which decreases with increasing programming temperature.

The recovery stage was carried out at 50°C, being the results shown in Figure 6A.

Different recovery behaviors can be observed in the graphs shown. The sample programmed at 40°C is activated earlier, presenting a stress peak in the early seconds of the test. This peak is related to the higher internal energy stored (after programming and fixing), and higher elastic behavior, which results in a faster recovery. After this peak, the stress values decrease at a fast rate, when compared to the remaining conditions, ending with the lowest value observed. This effect was already reported in the literature and occurs when the material attains its glass transition temperature.^[14]

On the contrary, samples programmed at higher temperatures (50 and 60°C), show a lower recovery energy

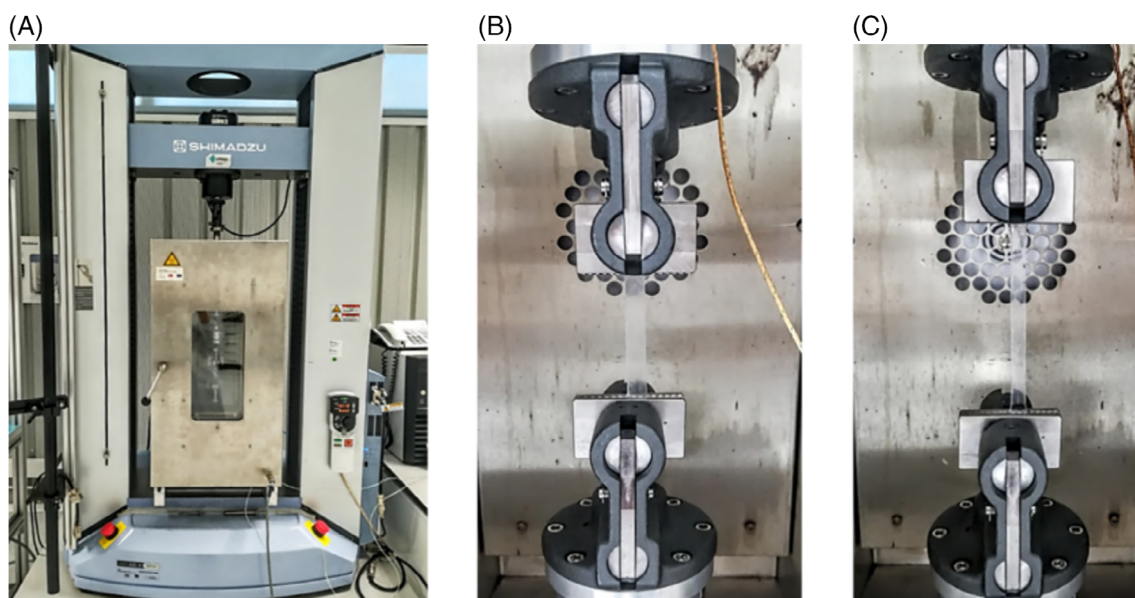


FIGURE 4 Constrained recovery tests: (A) tensile testing machine equipped with a heating chamber; (B) original sample before the programming stage; (C) sample after the constrained recovery stage

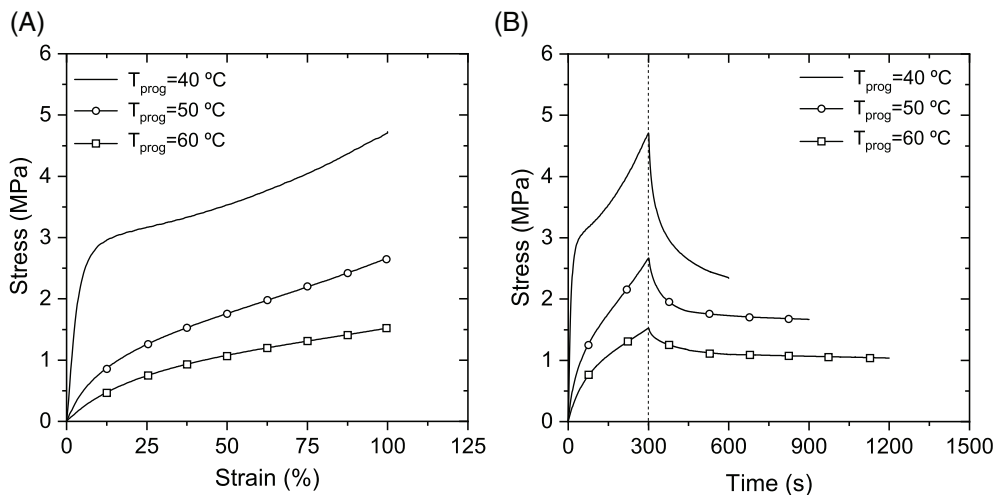


FIGURE 5 Effect of the programming temperature: (A) programming of the temporary shape (programming stage) carried out at different temperatures, at a deformation of $\epsilon_m = 100\%$; (B) complete stress-time curve, showing programming and fixing of the temporary shape (fixing stage), maintaining ϵ_m constant during the cooling until T_{fix} (30°C)

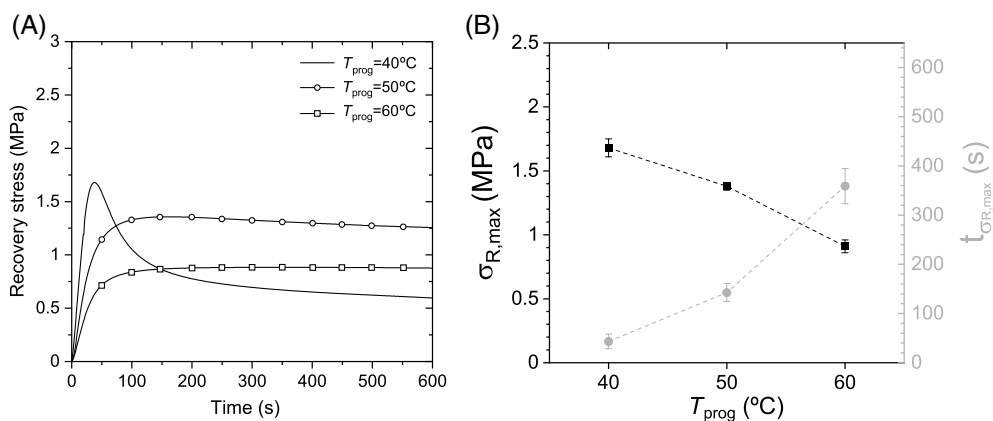


FIGURE 6 Constrained recovery, carried out at $T_{rec} = 50^\circ\text{C}$, of samples programmed at different T_{prog} : (A) stress-time recovery curves; (B) influence of T_{prog} on the maximum recovery stress, $\sigma_{R,max}$, and on the corresponding time, $t_{\sigma_{R,max}}$

(in-line with their lower stored energy), a slower recovery, and do not show a stress peak.

Figure 6B summarizes the effect of the programming temperature on the maximum recovery stress, $\sigma_{R,max}$, and on the corresponding recovery time, $t_{\sigma_{R,max}}$.

In Table 5, all the relevant results concerning the three stages (programming, fixing, and recovery) are listed, including the stress conversion ratios as defined by Equations 2 and 3. It can be seen that these ratios increase with increasing programming temperature, reaching, for 60°C , a value of 60% and 90% when the applied stress or the stored stress is considered, respectively. According to Wang et al.,^[62] deformations promoted below the glass transition temperature (as happens for the 40°C case) may originate the destruction of rigid domains, leading to irreversible deformation. This may justify the low values of the stress conversion ratios when programming is carried out at 40°C .

These results show that when using such SMP as an actuator, programming should be carried out at a temperature lower than T_{trans} when a high intensity, fast, but short duration reaction (recovery stress) is required; on

the other hand, if a lasting reaction is required, but at a lower intensity, programming should be performed at a temperature around T_{trans} .

5.2 | Influence of the maximum deformation

Figure 7 shows similar information as Figure 6, for the different deformations imposed at the programming stage (25%, 50%, 75% and 100%).

As expected, the stress required in the programming stage increases with the value of the imposed deformation. During the fixing stage, Figure 7B, the trend of the curves is similar, i.e., there is a direct relationship between the energy stored in the sample after cooling and the deformation imposed. The constrained recovery of these samples is shown in Figure 8A, performed at 50°C .

The trend of the recovery curves is also similar, and the activation time is of the same order of magnitude for all the deformations imposed. Also, the maximum stress

TABLE 5 Influence of T_{prog} (40, 50 and 60°C) on the parameters corresponding to the different stages of the thermo-mechanical cycle (programming, fixing and constrained recovery)

T_{prog} (°C)	Programming		Fixing	Recovery			
	σ_{100} (MPa)	E^a (MPa)	σ_m (MPa)	$\sigma_{R, \max}$ (MPa)	$t_{\sigma_{R, \max}}$ (s)	$\frac{\sigma_{R, \max}}{\sigma_{100}}$	$\frac{\sigma_{R, \max}}{\sigma_m}$
40	4.77 ± 0.10	60.92 ± 20.13	2.45 ± 0.12	1.68 ± 0.07	47.33 ± 14.64	0.36 ± 0.02	0.69 ± 0.03
50	2.68 ± 0.09	13.80 ± 2.67	1.70 ± 0.11	1.38 ± 0.03	142.67 ± 16.50	0.52 ± 0.01	0.82 ± 0.04
60	1.57 ± 0.07	3.54 ± 1.03	0.98 ± 0.05	0.91 ± 0.05	359.00 ± 35.61	0.58 ± 0.05	0.93 ± 0.03

^aYoung's modulus determined in the linear region of the stress-deformation curve.

FIGURE 7 Effect of the imposed deformation during the programming stage: (A) programming of the temporary shape (programming stage) carried out at different deformations, at $T_{\text{prog}} = 50^\circ\text{C}$; (B) complete stress-time curve, showing the fixing of the temporary shape (fixing stage), maintaining ϵ_m constant during the cooling until T_{fix} (30°C)

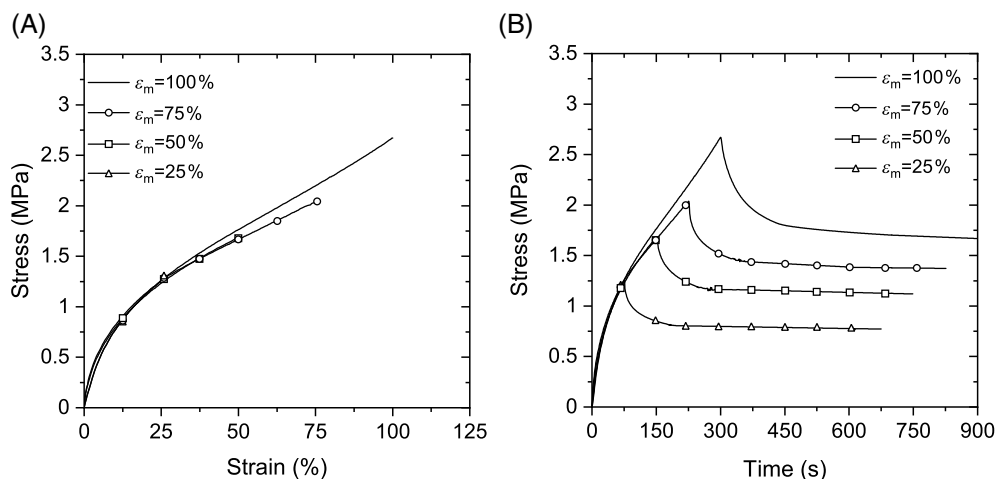
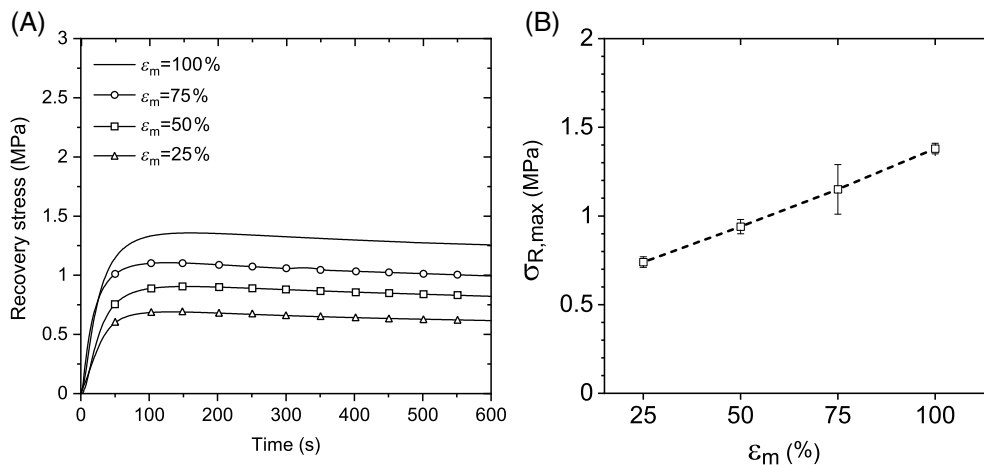


FIGURE 8 Constrained recovery, carried out at $T_{\text{rec}} = 50^\circ\text{C}$, of the samples programmed at different ϵ_m : (A) stress-time recovery curves; (B) influence of ϵ_m on the maximum recovery stress, $\sigma_{R, \max}$



stored after the fixing stage increases linearly with increasing deformation. The stress conversion ratios, depicted in Table 6, are similar, varying between 78% and 85% of the stored energy.

From a project design perspective, such results show that: (i) the stress available (released) in the recovery stage can be tuned in the programming stage through the value of the deformation imposed, and (ii) that the reaction time has not a strong dependence on the deformation imposed.

5.3 | Influence of the recovery temperature

The results corresponding to different recovery temperatures are illustrated in Figure 9.

All the samples were programmed and fixed in the same conditions and, therefore, the same level of energy was stored during the programming stage.

The recovery stress curve corresponding to 60°C, i.e. a temperature higher than T_{trans} , and also higher than the

TABLE 6 Influence of ϵ_m (25%, 50%, 75% and 100%) on the parameters corresponding to the different stages of the thermo-mechanical cycle (programming, fixing and constrained recovery)

ϵ_m (%)	Programming	Fixing	Recovery			
	$\sigma_{(\epsilon_m)}$ (MPa)	σ_m (MPa)	$\sigma_{R, \max}$ (MPa)	$t_{\sigma_{R, \max}}$ (s)	$\frac{\sigma_{R, \max}}{\sigma_{(\epsilon_m)}}$	$\frac{\sigma_{R, \max}}{\sigma_m}$
25	1.30 ± 0.16	0.87 ± 0.03	0.74 ± 0.03	118.00 ± 19.44	0.56 ± 0.01	0.84 ± 0.01
50	1.70 ± 0.02	1.11 ± 0.01	0.94 ± 0.04	167.67 ± 5.31	0.55 ± 0.03	0.85 ± 0.03
75	2.13 ± 0.10	1.47 ± 0.14	1.15 ± 0.14	127.00 ± 18.38	0.54 ± 0.04	0.78 ± 0.04
100	2.68 ± 0.09	1.70 ± 0.11	1.38 ± 0.03	142.67 ± 16.50	0.52 ± 0.01	0.82 ± 0.04

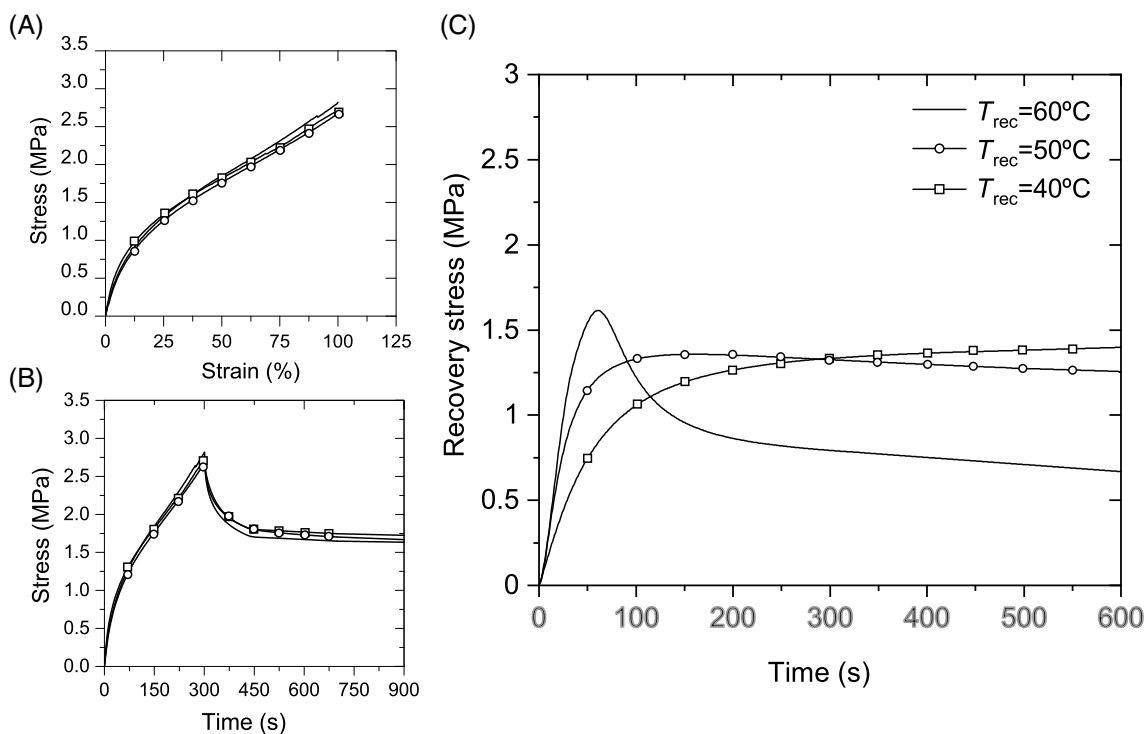


FIGURE 9 Effect of the recovery temperature, T_{rec} , in samples programmed at 50°C with an imposed deformation of 100%: (A) stress-deformation curves during the programming stage (B) evolution of stress over time in the programming and fixing stages; (C) stress along time in the constrained recovery stage

programming temperature, exhibits a peak in the initial phase of the recovery stage, which then drops until values lower than those corresponding to the remaining recovery temperatures. In contrast, at a recovery temperature lower than T_{trans} (40°C), the recovery stress increases continuously, at a low rate, over time. At T_{trans} , 50°C , the recovery shows an intermediate behavior. Having in mind the graph shown in Figure 10, it can be concluded that the maximum stress released is almost independent of the recovery conditions, which was expected since the stored stress during programming was also the same. What changes is the time required to reach this stress, which decreases with increasing temperature as a consequence of the progressive increase in molecular mobility.

As can be seen in Table 7, the stress conversion ratios are higher for the higher temperature tested, 60°C .

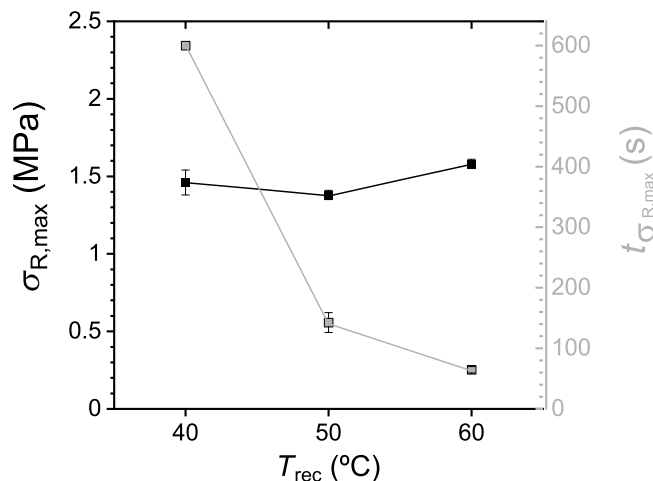


FIGURE 10 Effect of the recovery temperature on σ_{\max} and $t_{\sigma_{\max}}$

Again, the information gathered is important in the development of new applications, since T_{rec} enables to control the way the material releases the stress along time.

After this set of tests, the following project guidelines can be drawn: (i) to get a rapid, but low duration reaction (recovery stress), recovery should be carried out at a temperature higher than T_{trans} ; and (ii) if a lasting reaction is required, recovery should be performed at a temperature around T_{trans} . This is in line with the results obtained in Section 5.1., devoted to the effect of the programming temperature.

5.4 | Influence of the manufacturing process

In this final case study, the recovery behavior of samples produced by the FFF technique (3D printing)

was compared with that of samples produced by compression molding, when subjected to the same (reference) conditions during the programming and recovery stages.

Figure 11 shows information similar to that of the previous studies.

It can be seen that the samples produced by compression molding have better mechanical properties, requiring higher stresses to attain the imposed deformation and showing higher recovery stresses than those produced by 3D printing. The first occurrence was already expected, based on the previous experience on this subject.^[60,63] In fact, due to the well-known weaknesses promoted by poor bonding between the extruded filaments (in the same layer and in successive layers), and to the existence of voids, the mechanical performance of FFF printed samples is generally lower than that of molded

TABLE 7 Influence of the recovery temperature on the maximum stress released during the recovery stage and on stress conversion ratios

T_{rec} (°C)	$\sigma_{R, \text{max}}$ (MPa)	$t_{\sigma_{R, \text{max}}}$ (s)	$\frac{\sigma_{R, \text{max}}}{\sigma_{(\epsilon_m)}}$	$\frac{\sigma_{R, \text{max}}}{\sigma_m}$
40	1.46 ± 0.08	600.00 ± 0.00	0.54 ± 0.02	0.86 ± 0.03
50	1.38 ± 0.03	142.67 ± 16.50	0.52 ± 0.01	0.82 ± 0.04
60	1.58 ± 0.03	64.67 ± 5.19	0.57 ± 0.02	0.93 ± 0.01

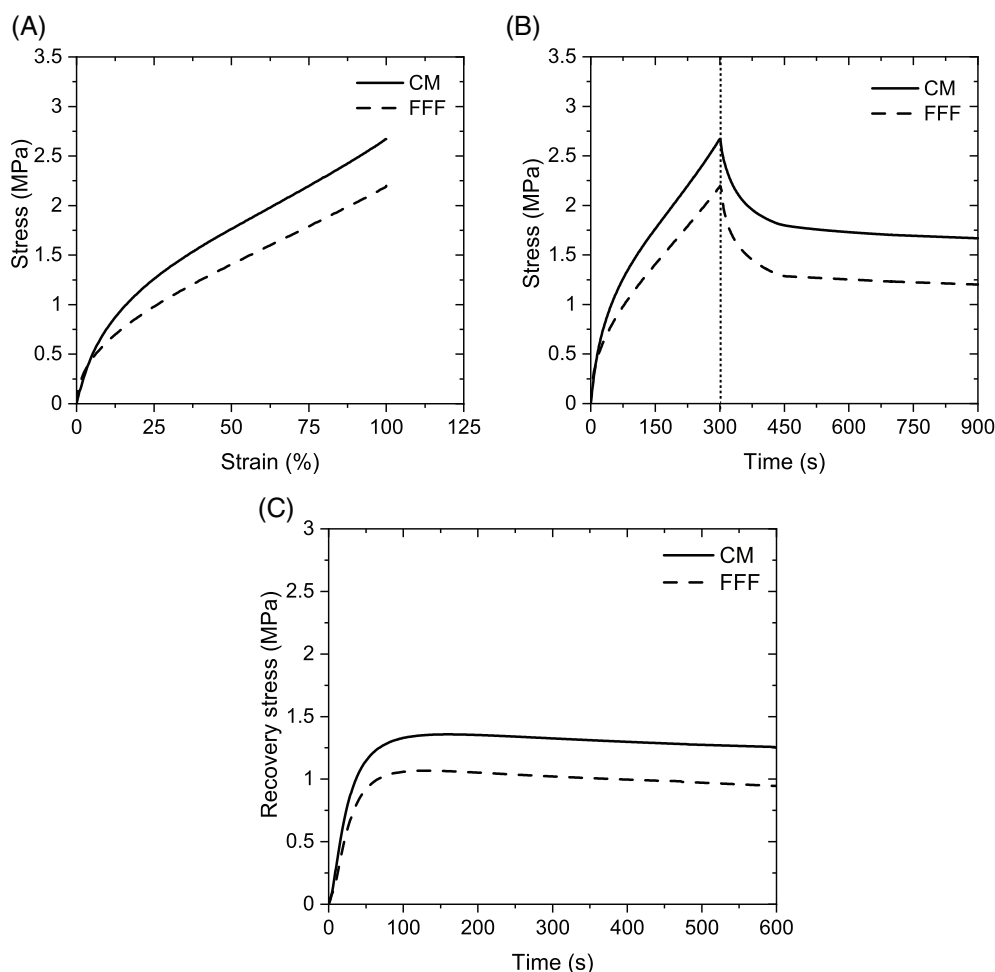


FIGURE 11 Influence of the samples manufacturing process (compression molding, CM, and 3D printing, FFF): (A) stress-deformation curves during the programming stage; (B) stress over time during the programming and fixing stages; (C) constrained recovery

TABLE 8 Influence of the manufacturing process used to produce the samples (compression molding, CM, and 3D printing, FFF) on the parameters corresponding to the programming and constrained recovery stages

Manuf. process	Programming	Fixing	Recovery			
	σ_{100} (MPa)	σ_m (MPa)	$\sigma_{R, \max}$ (MPa)	$t_{\sigma_{R, \max}}$ (s)	$\frac{\sigma_{R, \max}}{\sigma_{100}}$	$\frac{\sigma_{R, \max}}{\sigma_m}$
CM	2.68 ± 0.09	1.70 ± 0.11	1.38 ± 0.03	142.67 ± 16.50	0.52 ± 0.01	0.82 ± 0.04
FFF	2.16 ± 0.16	1.22 ± 0.06	1.03 ± 0.03	131.33 ± 3.40	0.48 ± 0.02	0.84 ± 0.03

counterparts. However, the most relevant finding is that the shape memory behavior of the material is not directly affected by 3D printing, since the stress conversion ratios, shown in Table 8, are maintained.

Based on the results, one can hypothesize that:

- the shape memory behavior of printed samples is expected to be similar to that presented by parts produced by conventional molding;
- the effect of the remaining parameters studied in this work (programming temperature, programming deformation, and recovery temperature) are, therefore, expected to apply to samples produced by 3D printing;
- in order to minimize the drawbacks inherent to 3D printed parts (poor adhesion between filaments and existence of voids), the printing conditions should be optimized if the level of the recovery stresses to be attained is intended to be similar to those observed in molded parts.

6 | CONCLUSION

The focus of the present research work was to provide quantitative data on the constrained recovery of SMP along time, due to the relevance of the topic in the development of actuators. The final purpose was, therefore, to provide relevant quantitative data and guidelines for the design of new applications employing SMP parts produced by molding techniques or 3D printing.

For this sake, a testing methodology was developed and used to assess the effect of some of the main parameters on the behavior of a SMP under constrained recovery, namely: the programming temperature, the deformation imposed at the programming stage, the recovery temperature, and the manufacturing method used in the production of the test samples. The selection of the relevant test temperatures was done after characterization of the glass transition temperature of the SMP (which was found to be around 50°C), a thermoplastic polyurethane.

In what concerns to the programming temperature, it was concluded that the maximum recovery stress diminishes with increasing temperature, and that the time

required to attain this value varies in the opposite way. Also, the maximum value of the stress conversion ratio (93%) was obtained for the higher programming temperature (60°C).

The effect of the deformation imposed in the programming stage (varied between 25% and 100%) showed that, in this range, the recovery stress is proportional to the deformation imposed, having almost no effect on the reaction time or stress conversion ratios.

The effect of the recovery temperature is, in some way, the opposite of that of the programming temperature in what concerns to the time required to attain the maximum recovery stress. In fact, an increase in this temperature results in a shorter time required. On the other hand, the maximum recovery stress is almost independent of the recovery temperature.

Among all the conditions tested, the maximum value of the recovery stress varied between 0.74 and 1.68 MPa, a relatively high range that enables some versatility in future applications. Also, the activation of the recovery stress can be short or long, and the stress can be maintained over time or can rapidly relax.

The study performed with 3D-printed samples showed that this technique preserves the shape memory behavior of the material, despite originating a reduction of the stresses involved. This fact is due to the inherent lower mechanical performance of 3D-printed parts, promoted by limited bonding between adjacent filaments and existence of voids. Therefore, the conclusions taken from the compression-molded samples can be extended to the printed ones, but a new study is required in order to determine the effect of the printing conditions.

ACKNOWLEDGMENTS

This work was funded by National Funds through FCT—Portuguese Foundation for Science and Technology, References UIDB/05256/2020 and UIDP/05256/2020, and UIDB/04436/2020 and UIDP/04436/2020.

DATA AVAILABILITY STATEMENT

The raw/processed data required to reproduce these findings cannot be shared at this time due to technical or time limitations.

ORCID

Andrea Zille  <https://orcid.org/0000-0001-5299-4164>

Alexandre Ferreira da Silva  <https://orcid.org/0000-0002-0672-2894>

Olga Sousa Carneiro  <https://orcid.org/0000-0001-5384-0028>

REFERENCES

- [1] D. Safranski, J. Griffis, *Shape-Memory Polymer Device Design*, 1st ed., Elsevier, Oxford, UK **2017**.
- [2] C. Liu, H. Qin, P. T. Mather, *J. Mater. Chem.* **2007**, *17*, 1543.
- [3] L. Shuai, Z. Jun, C. Jianjun, Y. Ming, L. Xuepeng, J. Zhiguo, *Polym. Eng. Sci.* **2019**, *59*, E310.
- [4] K. Wang, S. Strandman, X. X. Zhu, *Front. Chem. Sci. Eng.* **2017**, *11*, 143.
- [5] J. Hu, S. Chen, *J. Mater. Chem.* **2010**, *20*, 3346.
- [6] Y. Liu, H. Du, J. Leng, *Smart Mater. Struct.* **2014**, *23*(2), 1.
- [7] A. Lendlein, S. Kelch, *Angew. Chem., Int. Ed.* **2002**, *41*, 2034.
- [8] J. Hu, *Shape Memory Polymers and Textiles*, 1st ed., Woodhead Publishing, Cambridge **2007**.
- [9] J. Leng, X. Lan, Y. Liu, S. Du, *Prog. Mater. Sci.* **2011**, *56*, 1077.
- [10] M. Imran Khan, M. M. Zagho, R. A. Shakoor, in *Smart Polymer Nanocomposites* (Eds: D. Ponnamma, K. K. Sadasivuni, J. J. Cabibihan, A.-A. Al-Maadeed), Springer, Cham, Switzerland **2017**, p. 281.
- [11] F. L. Ji, J. L. Hu, S. S.-Y. Chui, *Polym. Eng. Sci.* **2012**, *52*, 1015.
- [12] M. Sáenz-Pérez, J. M. Laza, J. García-Barrasa, J. L. Vilas, L. M. León, *Polym. Eng. Sci.* **2018**, *58*(2), 238.
- [13] T. Sauter, M. Heuchel, K. Kratz, A. Lendlein, *Polym. Rev.* **2013**, *53*(1), 6.
- [14] K. Gall, C. M. Yakacki, Y. Liu, R. Shandas, N. Willett, K. S. Anseth, *J. Biomed. Mater. Res., Part A* **2005**, *73*(3), 339.
- [15] C. Azra, C. J. G. Plummer, J. A. E. Månson, *Smart Mater. Struct.* **2011**, *20*(8), 82002.
- [16] A. R. Damanpack, M. Bodaghi, W. H. Liao, *Smart Mater. Struct.* **2020**, *29*(8), 085016. <https://doi.org/10.1088/1361-665X/ab883a>
- [17] M. Bodaghi, A. Serjouei, A. Zolfagharian, M. Fotouhi, H. Rahman, D. Durand, *Int. J. Mech. Sci.* **2020**, *173*, 105451. <https://doi.org/10.1016/j.ijmecsci.2020.105451>
- [18] R. Noroozi, M. Bodaghi, H. Jafari, A. Zolfagharian, M. Fotouhi, *Polymers (Basel)* **2020**, *12*(3), 519. <https://doi.org/10.3390/polym12030519>
- [19] J. Raasch, C. Ayranci, D. Aldrich, M. Ivey, D. S. Nobes, *Addit. Manuf.* **2015**, *8*, 132.
- [20] C. A. Garcia Rosales, H. Kim, M. F. Garcia Duarte, L. Chavez, M. Castaneda, T.-L. B. Tseng, Y. Lin, *Rapid Prototyping J.* **2019**, *25*(2), 322.
- [21] S. Yamamura, F. Iwase, *Mater. Design* **2021**, *203*, 109605. <https://doi.org/10.1016/j.jmatdes.2021.109605>
- [22] E. A. Keneth, R. Lieberman, M. Rednor, G. Scalet, F. Auricchio, S. Magdassi, *Polymer* **2020**, *12*, 710. <https://doi.org/10.3390/polym12030710>
- [23] S. Valvez, P. N. B. Reis, L. Susmel, F. Berto, *Polymer* **2020**, *13*, 701. <https://doi.org/10.3390/polym13050701>
- [24] H. Dumlu, A. Marquardt, E. M. Zirdehi, F. Varnik, Y. Shen, K. Neuking, G. Eggeler, *Materials* **2021**, *14*, 481. <https://doi.org/10.3390/ma14030481>
- [25] G. Ehrman, A. Ehrman, *Polymer* **2021**, *13*, 164. <https://doi.org/10.3390/polym13010164>
- [26] G. Ehrman, A. Ehrman, *Polymer* **2021**, *13*, 1275. <https://doi.org/10.3390/polym13081275>
- [27] J. Leng, S. Du Eds., *Shape-Memory Polymers and Multifunctional Composites*, Taylor and Francis Group, New York **2010**.
- [28] M. Ahmad, J. Luo, B. Xu, H. Purnawali, P. J. King, P. R. Chalker, Y. Fu, W. Huang, M. Miraftab, *Macromol. Chem. Phys.* **2011**, *212*(6), 592.
- [29] S. Farzaneh, J. Fitoussi, L. Albert, B. Michel, A. Tcharkhtchi, *J. Appl. Polym. Sci.* **2013**, *5*(128), 3240.
- [30] W. M. Huang, B. Yang, Y. Q. Fu, *Polyurethane Shape Memory Polymers*, 1st ed., CRC Press, Boca Raton, FL **2011**.
- [31] F. Li, J. Hou, W. Zhu, X. Zhang, M. Xu, X. Luo, D. Ma, B. K. Kim, *J. Appl. Polym. Sci.* **1996**, *62*(4), 631.
- [32] J. H. Yang, B. C. Chun, Y. C. Chung, J. H. Cho, *Polymer (Guildf)* **2003**, *44*(11), 3251.
- [33] Z. G. Wei, R. Sandstrom, S. M. Miyazaki, *J. Mater. Sci.* **1998**, *33*, 3743.
- [34] I. A. Rousseau, *Polym. Eng. Sci.* **2008**, *48*, 2075.
- [35] C. Schmidt, A. M. Sarwaruddin Chowdhury, K. Neuking, G. Eggeler, *J. Polym. Res.* **2011**, *18*(6), 1807.
- [36] D. Santiago, F. Ferrando, S. De La Flor, *J. Mater. Eng. Perform.* **2014**, *23*(7), 2561.
- [37] J. Cui, K. Kratz, A. Lendlein, *Smart Mater. Struct.* **2010**, *19*(6), 065019.
- [38] J. Cui, K. Kratz, M. Heuchel, B. Hiebl, A. Lendlein, *Polym. Adv. Technol.* **2011**, *22*(1), 180.
- [39] J. Cui, K. Kratz, A. Lendlein, *Mater. Res. Soc.* **2009**, *1193*, 2.
- [40] A. Lendlein, S. Kelch, *Clin. Hemorheol. Microcirc.* **2005**, *32*(2), 105.
- [41] E. A. Pieczyska, M. Maj, K. Kowalczyk-Gajewska, M. Staszczak, L. Urbanski, H. Tobushi, S. Hayashi, M. Cristea, *J. Mater. Eng. Perform.* **2014**, *23*(7), 2553.
- [42] H. Tobushi, T. Hashimoto, S. Hayashi, E. Yamada, *J. Intell. Mater. Syst. Struct.* **1998**, *9*(2), 127.
- [43] H. Tobushi, S. Hayashi, K. Hoshio, Y. Makino, N. Miwa, *J. Intell. Mater. Syst. Struct.* **2006**, *17*(12), 1075.
- [44] F. Li, F. Scarpa, X. Lan, L. Liu, Y. Liu, J. Leng, *Compos. Part A Appl. Sci. Manuf.* **2019**, *116*, 169.
- [45] H. Tobushi, K. Okumura, M. Endo, S. Hayashi, *J. Intell. Mater. Syst. Struct.* **2001**, *12*, 283.
- [46] Z. Zhao, F. Peng, K. A. Cavicchi, M. Cakmak, R. A. Weiss, B. D. Vogt, *ACS Appl. Mater. Interfaces* **2017**, *9*(32), 27239.
- [47] E. A. Pieczyska, M. Maj, K. Kowalczyk-Gajewska, M. Staszczak, A. Gradys, M. Majewski, M. Cristea, H. Tobushi, S. Hayashi, *Smart Mater. Struct.* **2015**, *24*(4), 045043. <https://doi.org/10.1088/0964-1726/24/4/045043>
- [48] Y. Liu, K. Gall, M. L. Dunn, P. McCluskey, *Smart Mater. Struct.* **2003**, *12*(6), 947.
- [49] M. Fejos, G. Romhány, J. Karger-Kocsis, *J. Reinf. Plast. Compos.* **2012**, *31*(22), 1532.
- [50] L. Yahia, *Shape Memory Polymers for Biomedical Applications*, Woodhead Publishing, Sawston, UK **2015**.
- [51] J. Hu, *Advances in Shape Memory Polymers*, 1st ed., Woodhead Publishing, Philadelphia, PA **2013**.
- [52] R. Kazakevičiute-Makovska, S. Mogharebi, H. Steeb, G. Eggeler, K. Neuking, *Adv. Eng. Mater.* **2013**, *15*(8), 732.
- [53] B. Legendre, C. Guignol, N. Betz, B. Legendre, A. Le Moel, N. Yagoubi, *Nucl. Instrum. Methods Phys. Res., Sect. B* **2001**, *185*, 100.

- [54] T. K. Chen, J. Y. Chui, T. S. Shieh, *Macromolecules* **1997**, 30(17), 5068.
- [55] J. Balko, B. Fernández-D'Arías, E. Pöselt, R. Dabbous, A. J. Müller, T. Thurn-Albrecht, *Macromolecules* **2017**, 50(19), 7672.
- [56] R. E. Solís-Correa, R. Vargas-Coronado, M. Aguilar-Vega, J. V. Cauich-Rodríguez, J. San Román, A. Marcos, *J. Biomater. Sci., Polym. Ed.* **2007**, 18(5), 561.
- [57] T. Zapletalova, S. Michielsen, B. Pourdeyhimi, *J. Eng. Fiber. Fabr.* **2006**, 1(1), 62.
- [58] K. P. Menard, *Dynamic Mechanical Analysis: A Practical Introduction*, 1st ed., CRC Press, Boca Raton, USA **1999**.
- [59] C. M. Yakacki, S. Willis, C. Luders, K. Gall, *Adv. Eng. Mater.* **2008**, 10(1–2), 112.
- [60] O. S. Carneiro, A. F. Silva, R. Gomes, *Mater. Des.* **2015**, 83, 768.
- [61] M. H. Khaliq, R. Gomes, C. Fernandes, J. M. Nóbrega, O. S. Carneiro, L. L. Ferrás, *Rapid Prototyping J.* **2017**, 23(4), 727.
- [62] W. Wang, P. Ping, X. Chen, X. Jing, *Eur. Polym. J.* **2006**, 42(6), 1240.
- [63] A. E. Costa, A. F. Silva, O. S. Carneiro, *Rapid Prototyping J.* **2019**, 25(3), 555.

How to cite this article: C. Peixoto, A. Zille, A. Ferreira da Silva, O. S. Carneiro, *Polym. Eng. Sci.* **2021**, 1. <https://doi.org/10.1002/pen.25778>